Ceramics International **22** (1996) 143–147

0272-8842(95)00070-4
0272-8842/96/$15.00

Reactive Synthesis of AlN/TiB_2 Composite

G. J. Zhang & Z. Z. Jin

China Building Materials Academy, Beijing 100024, People's Republic of China

(Received 5 September 1994; accepted 10 March 1995)

Abstract: The phase-forming mechanisms in the chemical reaction 2Al + Ti + 2BN = TiB_2 + 2AlN have been investigated using X-ray diffraction. It is observed that several transient phases (such as $TiAl_3$, TiN and α-Al_2O_3) exist at different temperatures. It is suggested that the B_2O_3 in BN powder and oxygen absorbed by Al powder result in the forming of α-Al_2O_3 at temperatures below 1600°C. This α-Al_2O_3 will be reduced by the atmosphere in the graphite furnace and disappear at temperatures higher than 1700°C. Thus combining thermodynamic analysis, the synthesis temperature of AlN/TiB_2 must be above 1700°C. Further, the AlN/TiB_2 composite has been produced by reactive hot pressing at 1850°C under 25 MPa for 30 min in Ar atmosphere. The three-point bending strength and SENB fracture toughness are 539 MPa and 5·05 MPa·$m^{1/2}$, respectively. The residual stress in the composite caused by the considerable difference in thermal expansion between the AlN matrix and TiB_2 particles has been measured by XRD method. Combining crack propagation path analysis by SEM, the toughening mechanism of the composite is suggested to be thermal residual stress toughening and crack deflection toughening.

1 INTRODUCTION

AlN ceramic has good thermal conductivity and is considered for use as a high thermal conductivity substrate. It is also an attractive structural material, for example, sintered AlN polytype body with Y_2O_3–SiO_2 additive has a three-point bending strength of 700 MPa and K_{IC} of 5–7 MPa·$m^{1/2}$.[1] TiB_2 ceramic has good wear resistance and electrical conductivity, and is used for cutting tools and electrodes. Zdaniewski[2] proposed that TiB_2–AlN composite should be used to replace graphite cathodes in aluminum electrosmelting. He used TiB_2 and AlN powders as starting materials to produce TiB_2–AlN composite. In the present work, a reactive hot-pressing method based on the following chemical reaction was used to prepare AlN/TiB_2 composite.[3,4]

$$2Al + Ti + 2BN \rightarrow TiB_2 + 2AlN \qquad (1)$$

According to the above reaction, the volume contents of AlN and TiB_2 are calculated to be 62 and 38%, respectively.

In this paper, the phase-forming mechanism of the above reaction is discussed. The mechanical properties and microstructure of the AlN/TiB_2 composite produced by reactive hot pressing have been investigated. Finally, the thermal residual stresses and toughening mechanism are analysed.

2 EXPERIMENTAL PROCEDURES

The raw materials are powders of Al (< 10 μm), TiH_2 (< 40 μm) and BN (purity > 98%, B_2O_3 < 0·75%, particle size ~1 μm). The stoichiometrical powders were mixed and milled in alcohol (chemical purity) with Al_2O_3 balls for 12 h and then dried. The powder mixture was calcined at various temperatures ranging from 1000 to 1740°C in an Ar atmosphere for 30 min; the phase composition determination was done by X-ray diffraction. Afterwards, the AlN/TiB_2 composite was produced by reactive hot pressing (RHP) at 1850°C under 25 MPa in an Ar atmosphere for 30 min. The fracture strength was measured on bars (3 × 4 × 36 mm^3) machined from the hot-pressed specimen

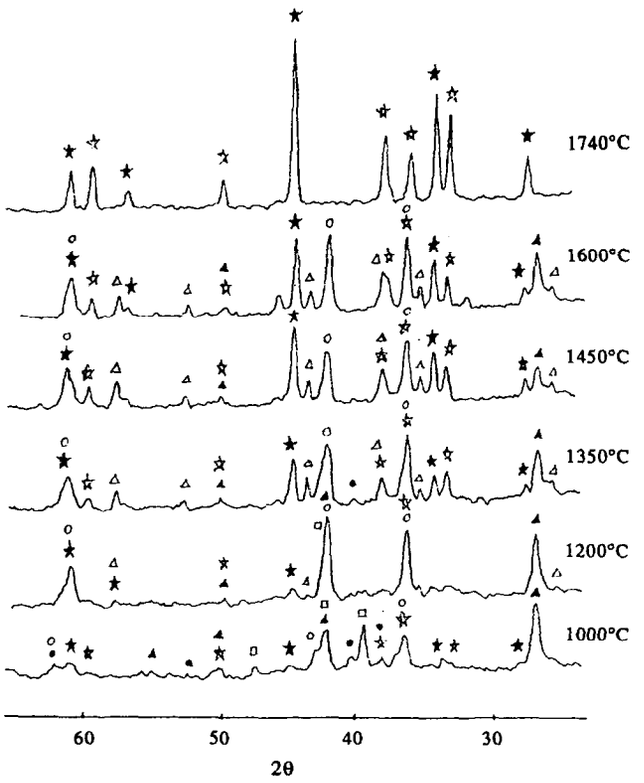

Fig. 1. XRD patterns of reaction (1) after calcining at different temperatures for 30 min in Ar atmosphere. ☆ AlN, ★ TiB_2, ● Ti, ○ TiN, Δ α–Al_2O_3, ▲ BN, □ $TiAl_3$

by a three-point bending method and fracture toughness on samples ($2 \times 4 \times 20$ mm^3) by SENB method. The crosshead speed was 0·5 mm/min. Microstructure and crack propagation path were examined by SEM. The residual stress in the AlN/TiB_2 composite was measured by X-ray diffraction.

3 REACTION MECHANISMS

Figure 1 is the XRD pattern of the powder mixture after calcining at different temperatures. The phase composition is summarized in Table 1. It can be seen that there are different transient phases existing at different temperatures. The phase forming process is suggested to be as follows:

$$TiH_2 \rightarrow Ti + H_2\uparrow$$
$$3Al + Ti \rightarrow TiAl_3$$
$$3Ti + 2BN \rightarrow 2TiN + TiB_2$$
$$3TiN + TiAl_3 \rightarrow 3AlN + 4Ti$$

Table 1. Phase composition of reaction (1) at various temperatures

Temperature (°C)	Phase composition
1000	BN, TiN, $TiAl_3$, TiB_2, AlN, Ti
1200	TiN, BN, TiB_2, AlN, $TiAl_3$, Ti, α–Al_2O_3
1350	TiN, BN, TiB_2, AlN, α–Al_2O_3, Ti
1450	TiB_2, TiN, AlN, α–Al_2O_3, BN
1600	TiB_2, TiN, AlN, BN, α–Al_2O_3
1740	TiB_2, AlN

The B_2O_3 existed in the BN powder and oxygen absorbed by the Al powder results in the formation of α–Al_2O_3 at a temperature range between 1200 and 1600°C:

$$3B_2O_3 + 2TiAl_3 + Ti \rightarrow 3\alpha\text{–}Al_2O_3 + 3TiB_2$$
$$2TiAl_3 + \frac{9}{2}O_2 \rightarrow 3\alpha\text{–}Al_2O_3 + 2Ti$$

However, α–Al_2O_3 will be reduced by the reducing atmosphere in the furnace with graphite die and heaters at higher temperatures and then react with the remainder of BN and TiN. So the following reactions are suggested:

$$Al_2O_3 + 3C \rightarrow 2Al + 3CO\uparrow$$
$$Al + TiN \rightarrow AlN + Ti$$
$$3Ti + 2BN \rightarrow 2TiN + TiB_2$$

The overall reaction is:

$$3Al_2O_3 + 9C + 4BN + 2TiN \rightarrow 2TiB_2 + 6AlN + 9CO\uparrow \quad (2)$$

The free enthalphy of the above reaction between 298 and 2000 K is (thermodynamic data refer to Ref. 5):

$\Delta G_T^0 = 772{\cdot}32 - 390{\cdot}615 \times 10^{-3}T$ (kcal)

when $\Delta G_T^0 = 0$, $T = 1977$ K $= 1704$°C; accordingly, this reaction will thermodynamically take place spontaneously at temperatures higher than 1704°C. This coincides with the experimental results. Taking place in a flow of Ar, in which the pressure of CO was far lower than the equilibrium pressure (1 atm), reaction (2) is shifted to the right.

4 MECHANICAL PROPERTIES AND MICROSTRUCTURE OF THE AlN/TiB_2 COMPOSITE

The mechanical properties are listed in Table 2. It can be seen that the K_{IC} is considerably higher than that of monolithic AlN ceramics (2·7 MPa·m$^{1/2}$).[2] Observation of the Vickers indentation crack (98 N) introduced on a polished surface revealed that the crack was deflected by TiB_2 particles, as shown in Fig. 2. Figure 3 is the SEM micrograph of the fractured surface, showing the existence of crack deflection. It was suggested that the crack propagation resistance is increased by both the crack deflection itself (crack deflection toughening[6]) and the residual stress (see Section 5)

Table 2. Properties of AlN/TiB_2 composite

Relative density (%)	Vickers hardness (GPa)	Bending strength (MPa)	Fracture toughness (MPa·m$^{1/2}$)
98·21	17·8 ± 1·5	539 ± 43	5·05 ± 0·31

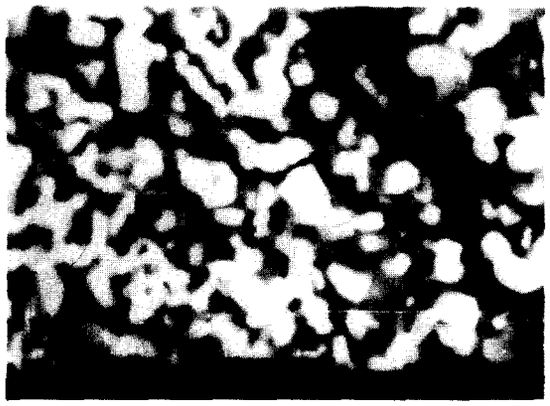

Fig. 2. Crack deflection in AlN/TiB_2 composite. The white range is TiB_2, the gray range is AlN.

Table 3. Characteristics of AlN and TiB_2.[7]

Phase	Young's modulus (GPa)	Poisson's ratio	CTE ($\times 10^{-6}$/°C)
AlN	350	0·25	4·03
TiB_2	529	0·28	8·10

in the matrix of AlN generated by the mismatch of thermal expansion coefficients (see Table 3[7]) of the AlN matrix and TiB_2 particles (residual stress toughening[8]), thus the K_{IC} is increased. Figure 4 shows a large agglomerate of TiB_2 unit particles on the fracture surface. The agglomerate might act as a fracture source by detaching from the AlN matrix when the temperature dropped from hot-pressing temperature to room temperature. Therefore it is important to eliminate the agglomeration by appropriate processing.

5 RESIDUAL STRESSES

For a particle in an infinite matrix, a hydrostatic stress P will be developed caused by the mismatch between the thermal expansion coefficients (α) and elastic moduli (E) of the matrix and the dispersed particle:[9]

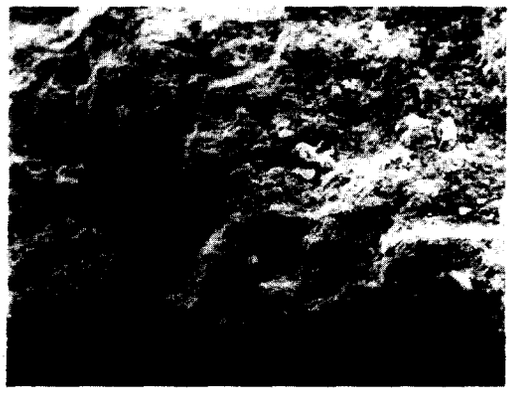

Fig. 3. Fractograph of AlN/TiB_2 composite by SEM.

Fig. 4. An agglomerate of TiB_2 particles observed in the fractured surface in AlN/TiB_2 composite.

$$P = \frac{2\Delta\alpha\Delta T E_m}{(1 + \upsilon_m) + 2\beta(1 - 2\upsilon_p)} \quad (3)$$

where the subscripts p and m refer to the particle and matrix, respectively. $\Delta\alpha = \alpha_p - \alpha_m$, $\beta = E_m/E_p$ and ΔT is the temperature range over which stresses are not relieved. In the AlN/TiB_2 composite produced by reactive hot pressing, AlN is treated as the matrix and TiB_2 as the second particulate phase. Using data given in Table 3 and setting ΔT = 1200 K, P = 1866 MPa was obtained. Thus the radial matrix stress σ_r ($= PR^3/r^3$) and the tangential matrix stress σ_t ($= -PR^3/2r^3$) will set up, where R is the particle radius and r is the distance from the centre of the particle. Obviously, the matrix stresses varying with $(R/r)^3$ are useful for analysing the crack propagation path,[10] but not convenient to calculate the toughening increment quantitatively. Taya *et al.*[8] proposed a method to calculate the average residual stresses in the composite. According to this method, the calculated average residual stresses for the AlN matrix and TiB_2 particles in AlN/TiB_2 composite are:

$$\left.\begin{aligned} \langle\sigma\rangle_{AlN} &= -639 \text{ MPa} \\ \langle\sigma\rangle_{TiB_2} &= 1045 \text{ MPa} \end{aligned}\right\} \quad (4)$$

respectively (not considering the effect of porosity). In the present work, these stresses were measured by X-ray diffraction. The specimen for residual stress measurement was carefully ground. XRD analysis was performed with FeK_α radiation at 40 keV and 20 mA, and DS = 1°, RS = 1·5° and SS = 1°. The beam size at the sample was approximately 0·5 × 1·0 cm^2. The reflections used were the (203) (2θ = 135·5°) for AlN and the (112) (2θ = 122·4°) for TiB_2, as shown in Fig. 5. Figure 6 shows the coordinate system used for residual stress determination, where S_i are the sample coordinates and L_i are the laboratory coordinates. In the present work, we assumed σ_3 = 0 and

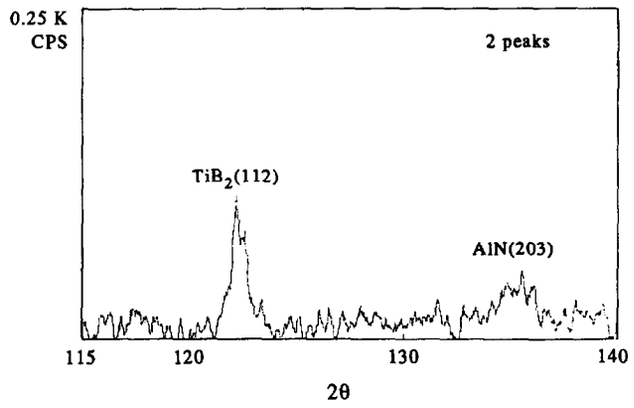

Fig. 5. X-ray diffraction intensity peaks used for residual stress measurements.

ignored the effect of any shear stress. The XRD method is based on the measurement of $2\theta_\psi$ at various angles of incident beam tilt ϕ and ψ as shown in Fig. 6. The stress σ_ϕ in S_ϕ direction, which was selected to be vertical to the grinding direction, is the average macrostress $<\sigma>$ in demand and was calculated by:[11]

$$<\sigma> = \sigma_\phi = \frac{-E}{2(1+\nu)} \operatorname{ctg} \theta_0 \frac{\pi}{180} \left(\frac{\partial(2\theta_\psi)}{\partial(\sin^2\psi)} \right) \quad (5)$$

where E,ν are Young's modulus and Poisson's ratio for the particular phase, $2\theta_0$ is the diffraction angle of the same peak in a non-stressed sample and can be replaced by theoretical datum. $\frac{\partial(2\theta_\psi)}{\partial(\sin^2\psi)}$ is the slope of the line $2\theta_\psi - \sin^2\psi$. The X-ray measurements of $2\theta_\psi$ yield the total stress $<^t\sigma>$ of each phase, including the eigenstress $<\sigma>$ of each phase resulting from thermal expansion mismatch and the residual stress $<\sigma^m>$ induced by machining:

$$<^t\sigma>_{AlN} = <\sigma>_{AlN} + <\sigma^m> \quad (6)$$

$$<^t\sigma>_{TiB_2} = <\sigma>_{TiB_2} + <\sigma^m> \quad (7)$$

The eigenstresses must sum to zero, i.e.[12]

$$(1-f)<\sigma>_{AlN} + f<\sigma>_{TiB_2} = 0 \quad (8)$$

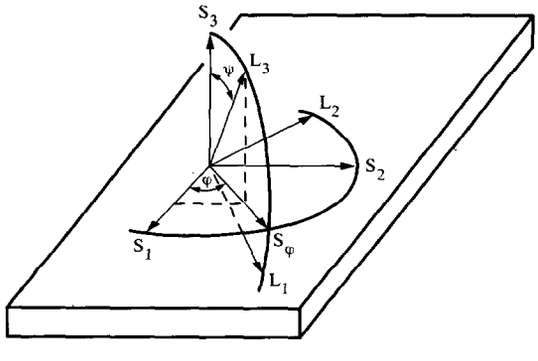

Fig. 6. Coordinate system used in residual stress determination. S_i – sample coordinate, L_i – laboratory coordinate.

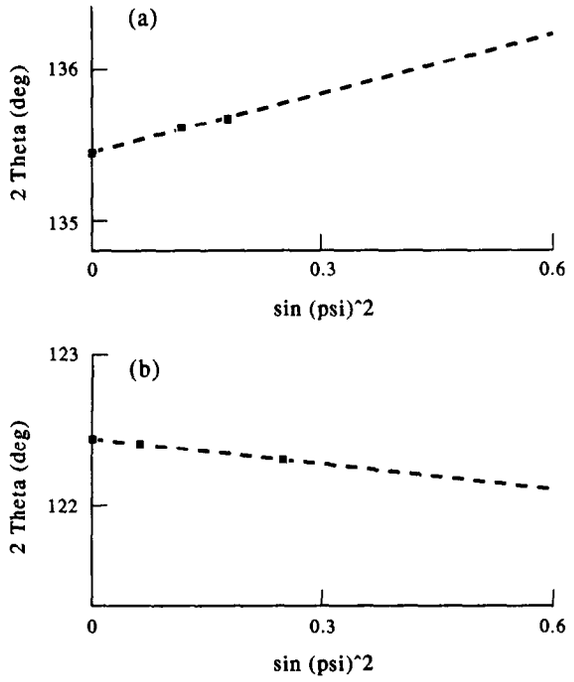

Fig. 7. Relationship between $2\theta_\psi$ and $\sin^2\psi$ (a) for AlN and (b) for TiB_2.

where f (= 38%) is the volume fraction of the TiB_2 phase. Solving eqns (6), (7) and (8), one can obtain $<\sigma>_{AlN}$, $<\sigma>_{TiB_2}$ and $<\sigma^m>$. With increase of ψ, the penetration-depth of the X-ray beam into the sample surface will decrease and the fraction of the surface residual stress induced by machining will increase, which will affect the linear relationship between $2\theta_\psi$ and $\sin^2\psi$. So the angle ψ should be kept less than 30°.

Figure 7 shows the linear relationship of $2\theta_\psi$ and $\sin^2\psi$ for AlN and TiB_2 in the AlN/TiB_2 composite. Using eqn (5) and substituting relative data from Table 3, we obtained:

$$\left.\begin{aligned} <^t\sigma>_{AlN} &= -100{\cdot}06 \text{ MPa} \\ <^t\sigma>_{TiB_2} &= 164{\cdot}44 \text{ MPa} \end{aligned}\right\} \quad (9)$$

and

$$\left.\begin{aligned} <\sigma>_{AlN} &= -100{\cdot}35 \text{ MPa} \\ <\sigma>_{TiB_2} &= 164{\cdot}15 \text{ MPa} \\ <\sigma^m> &= 0{\cdot}29 \text{ MPa} \end{aligned}\right\} \quad (10)$$

It can be seen that some tensile residual stress vertical to the grinding direction will be induced by grinding. The average measured eigenstresses of AlN and TiB_2 are only 16% of the theoretical values (see eqn (4)). Two main possibilities were suggested: (1) Residual stresses measured by XRD method are only the stresses near the surface. The eigenstress is seriously affected by the free surface; (2) some TiB_2 agglomerates may spontaneously crack on cooling (see Fig. 4). Nevertheless, the results show that there was considerable residual compressive stress in the AlN matrix and tensile stress in TiB_2 particles. These results support the residual stress toughening mechanism and crack deflection toughening

mechanism in the AlN/TiB_2 composite produced by reactive hot pressing as discussed in Section 4.

6 CONCLUSIONS

(1) Several transient phases such as $TiAl_3$, TiN and α–Al_2O_3 existed in the reaction of TiH_2, Al and BN at different temperatures. Thermodynamic calculation showed that the synthesis temperature of reaction Al + Ti + BN to produce AlN/TiB_2 composite should be higher than 1700°C.

(2) The bending strength and fracture toughness of AlN/TiB_2 composite prepared by reactive hot pressing at 1850°C under 25 MPa in Ar atmosphere for 30 min were 539 MPa and 5·05 MPa·$m^{1/2}$.

(3) The thermal residual stresses of AlN and TiB_2 phases in the composite were analysed and then measured by XRD. It was suggested that the main toughening mechanisms of the composite were thermal residual stress toughening and crack deflection toughening.

REFERENCES

1. KOMEYA, K., Aluminum nitride ceramics — historical review and future trend. *Ceram. Japan*, **26** (1991) 725–32.
2. ZDANIEWSKI, W. A., Stereoscopic fractography of crack propagation phenomena in a TiB_2–AlN composite. *J. Am. Ceram. Soc.*, **72**, (1989) 116–21.
3. ZHANG, G. J., Preparation of multiphase ceramic composites by reactive hot pressing. *Proceedings of the China National 4th Annual Conference on Advanced Ceramics*, Chinese Ceramic Society, Beijing, 1992, 29–31.
4. ZHANG, G. J. & LI, Y. P., Preparation and toughening mechanism of AlN/TiB_2 particulate composite by reactive hot pressing. *Proceedings of the 5th International Symposium on Ceramic Materials and Components for Engines*, Shanghai, 29 May – 1 June 1994, pp. 322–5.
5. YE. D. L., *Handbook of Thermodynamic Data for Inorganic Materials*. Metallurgical Industry Publisher, Beijing, 1981, pp. 73, 77, 112, 171, 195, 978, 982.
6. FABER, K. T. & EVANS, A. G., Crack deflection processes —I. Theory. *Acta Metall.*, **31** (1983) 565–76.
7. South China Institute of Technology *et al.* (ed.), *Technology of Ceramics*. China Architectural Industry Publisher, Beijing, 1981, p. 390.
8. TAYA, M., HAYASHI, S., KOBAYASHI, A. S. & YOON, H. S., Toughening of particulate-reinforced ceramic-matrix composite by thermal residual stress. *J. Am. Ceram. Soc.*, **73** (1990) 1382–91.
9. ZHANG, G. J. & JIN, Z. Z., Toughening mechanisms of particulate composite ceramics. *J. Chinese Ceram. Soc.*, **22** (1994) 259–69.
10. ZHANG. G. J., YUE, X. M. & JIN, Z. Z., Microprocesses of crack propagation in particulate toughening ceramics. *J. Chinese. Ceram. Soc.*, **23** (1995) 365–72.
11. FAN, X., *X-Ray Technique for Metals*. Mechanical Industry Publisher, Beijing, 1981, p. 127.
12. MAGLEY, D. G., WINHOLTZ, R. A. & FABER, K. T., Residual stresses in a two-phase microcracking ceramic. *J. Am. Ceram. Soc.*, **73** (1990) 1641–4.